

Supplementary Information

The origin of discrete current fluctuations in a fresh single molecule junction

Dong Xiang,^{a,b} Takhee Lee,^{b,*} Youngsang Kim,^c Tingting Mei^a and Qingling Wang^{d,*}

^a Institute of Modern Optics, Nankai University, Key Laboratory of Optical Information Science and Technology, Ministry of Education, Tianjin 300071, China.

^b Department of Physics and Astronomy, Seoul National University, Seoul 151-747, Korea

^c Department of Mechanical Engineering, University of Michigan, Ann Arbor MI-48109, USA

^d Faculty of Mechanical and Electronics Information, China University of Geosciences, 430074, China

Table of Contents

1. Chip fabrication	2
2. Experimental setup	3
3. Calculation of the attenuation factor	4
3.1. Estimation by geometry of the setup	4
3.2. Calculation by the tunneling current	4
4. Measurement system	5
5. Noise spectroscopy of molecule free junction	6
6. Obtaining a single molecule junction by closing the gap size	7
7. Determination of the characteristic frequency	8
8. Noise characterization of molecule junctions with differing types of molecules	9
9. Telegram-like fluctuations on molecular incubation concentration	10
References	10

1. Chip fabrication

The chip fabrication process consists of five steps [S1-S5]: (1) A polyimide layer (3 μm thick) is spun on the substrate followed by a baking and annealing process; (2) 200 nm thick positive tone resist is spin coated onto the substrate and baked at 180 °C for 2 minutes. Then, the electrode patterns are written by the lithography system. Finally, a standard development procedure is applied before the substrate is immersed in 2-propanol to stop the development; (3) After development, the resist layer serves as a mask for the metal deposition. At this point, Ti (2 nm thick) and Au (40 nm thick) are deposited onto the substrate surface in a vacuum chamber; (4) After depositing the metals, the sample is immersed in acetone for lift off process; (5) In the final step, in order to obtain a suspended metallic bridge in the nanostructure area, the polyimide layer is isotropically etched by reactive ion etching in conditions of 32 sccm of oxygen and 8 sccm of CHF₃ with 100 W of power.

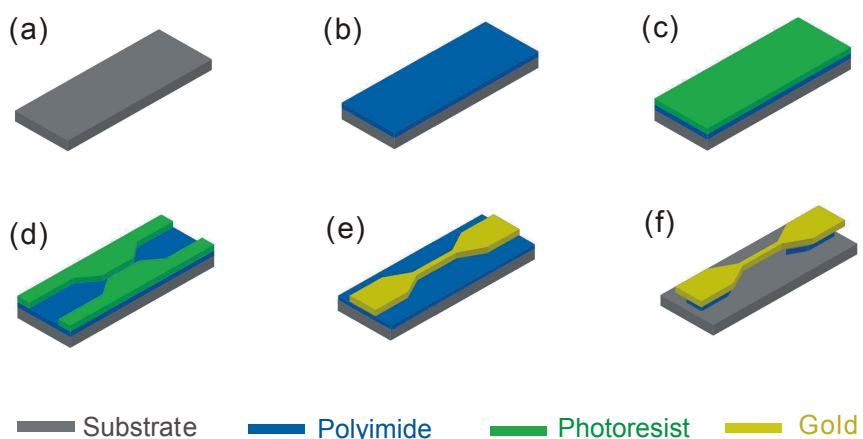


Fig. S1 Micro-fabrication process of MCBJ chips. (a) Spring steel was used as the substrate (named ‘bend beam’ in this text). (b) A polyimide layer (HD-4100, HD Microsystem), about 3 μm thick, is spun on the substrate. (c) Positive tone resist (PMMA) is spin coated onto the substrate and baked at 180 °C for 2 minutes. The electrode pattern is made by means of electron beam lithography. (d) A standard development procedure is applied to remove the resist exposed by the electron beam. (e) After deposition of the metals layer, the sample is immersed in acetone for lift off. (f) In the final step, to obtain a suspended metal bridge the polyimide is isotropically etched by reactive ion etching (RIE).

2. Experimental setup

A spring steel chip is mounted into a homemade three-point bending apparatus. The two outer posts of the three-point bending apparatus are fixed while the third one works as a push rod in the Z-direction (Fig. S2). All of the setup (except the push rod) is fabricated by steel to suppress unexpected deformation. Controlling the displacement of the push rod in the Z-direction facilitates bending or relaxation of the chip. Two different push rods were employed. The first kind is driven by a piezo actuator with high resolution and the second is moved by a differential screw with a step motor. The tiny pitch difference of the differential screw between S1(0.7mm/r) and S2(0.75mm/r) enables us to precisely control the movement of the push rod. When the motor rotates one turn, the displacement of the push rod is only $50\mu\text{m}$. When the push rod exerts a bending force on the substrate, the movement in the Z-direction causes an elongation of the constriction until the metal bridge breaks, resulting in two separated nanoscale electrodes.

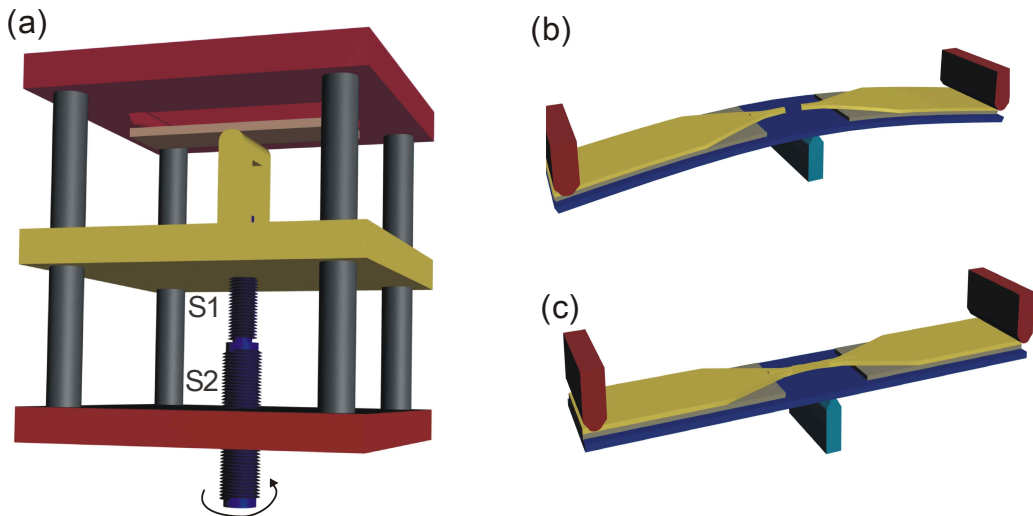


Fig. S2 MCBJ setup and push rods. **(a)** Schematics side-view of the MCBJ setup driven by a motor. The tiny pitch difference of the screw between S1 and S2 allows us to precisely control movement of the push rod. **(b)** Side-view of the MCBJ substrate after breaking the nano-constriction, correspondingly the substrate is in a bending configuration. **(c)** Side-view of the MCBJ substrate before breaking the nano-constriction.

3. Calculation of the attenuation factor

The attenuation factor is defined by the following formula: $r = \Delta X / \Delta Z$. Here, r is the attenuation factor, ΔX is the gap size change between the two nanoelectrodes and ΔZ is the displacement of the push rod. There are two methods to calculate the attenuation factor: (1) Calculation by the geometrical configuration of the system; (2) Calculation by measuring the tunneling current.

3.1. Estimation by the setup geometry

The attenuation factor can be estimated by the geometrical configuration of the setup [S6]. According to previous reports, it can be calculated as $r = \Delta X / \Delta Z = 6ut / L^2$, where u is the length of the suspended bridge, t is the thickness of the steel substrate and L is the length between the two outer posts above the spring steel substrate. In our case, we obtained $r = \Delta X / \Delta Z = 6ut / L^2 \approx 6 \times 0.8 \mu m \times 0.32 mm / (25 mm)^2 \approx 3 \times 10^{-6}$.

3.2. Calculation by the tunneling current

The attenuation factor can also be determined from the change of tunneling current as a function of the push rod displacement [S6]. At a low bias range, the tunneling current can be described by the following equation: $I \propto \exp(-2d\sqrt{2m\phi/\hbar})$. Here, d is the gap size, m is the electron mass and ϕ is the barrier height [S1, S7]. The attenuation factor can be calculated from the ratio: $r = \Delta X / \Delta Z$. The push rod displacement (ΔZ) can be measured directly and the corresponding gap size change (ΔX) can be extracted from the change in tunneling current curves. In our case, the value of the attenuation factor, r , was calculated to be 5×10^{-6} [S6].

4. Measurement system

The measurement setup is illustrated in Fig. S3. First, the bias voltage is applied to the sample via a lead-acid battery and a variable resistor. A capacitor is connected in parallel to the variable resistor to remove its influence on the measured spectra. When ‘conductance measurement mode’ is switched on, the single-molecule junction can be identified by monitoring conductance change during the separating process of the two electrodes. Under ‘noise measurement mode’, the spectrum analyser is operated in the cross-spectrum mode and performs the Fourier transform of the cross-correlated signal followed by two pre-amplifiers over a bandwidth from 1 Hz to 100 kHz. All the measurements were carried out in vacuum at less than 10^{-3} mbar and at room temperature.

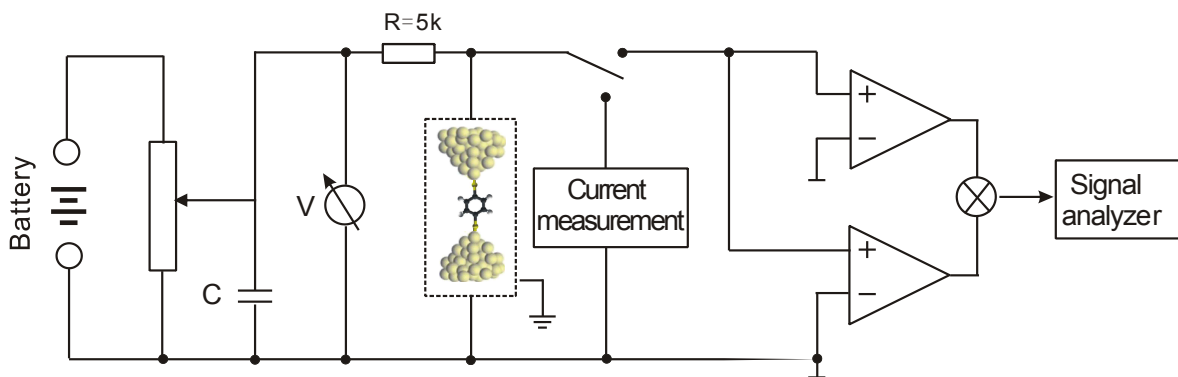


Fig.S3 The schematic drawing of noise and real-time current measurement system. The operation mode can be switched between ‘current measurement mode’ and ‘noise measurement mode’. The monopole double throw switch can be turned downwards to connect the current measurement device, or turned upwards to connect the spectroscopy measurement system. After a single-molecule junction was identified and real-time current measurement was performed, the setup was switched to ‘noise measurement mode’.

5. Characterization of molecule-free junctions

The noise characteristics of bare metal break junctions were previously investigated in detail from the diffusive to the ballistic transport regime.⁵⁵ Here, we focus our attention on investigating the noise properties of MCBJ samples in the tunneling regime. The molecule-free nanogap is used as a reference system for molecule-containing junctions. Voltage fluctuations were measured and Fourier transformed using a dynamic signal analyzer. The voltage power noise spectral density, S_V , was measured over a bandwidth from 1Hz to 100 kHz at different gap dimensions. For all gap dimensions, the spectra mainly follow $1/f$ noise behavior ($1.0 \leq \alpha < 1.2$).

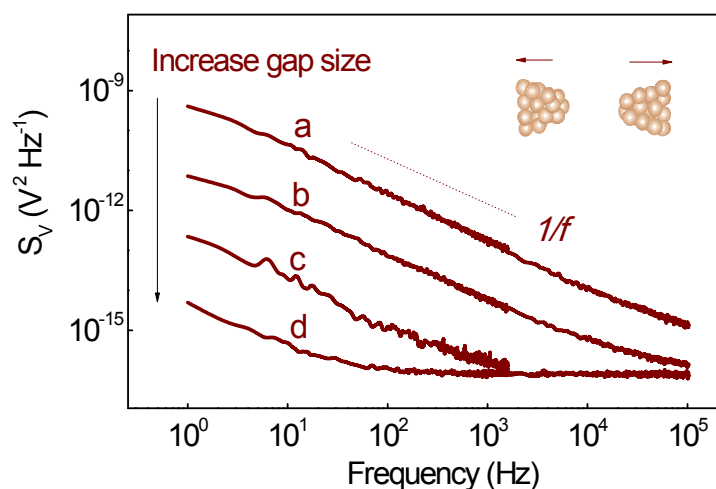


Fig. S4 The voltage noise power spectral density of the molecule-free junctions in the tunneling regime with increasing gap size (a-d) between bare gold nanoelectrodes. The fixed bias voltage applied to the junction is $V_B = 0.1$ V. The horizontal black line represents the theoretically calculated thermal noise ($4kT$). For small gap dimensions, the spectra follow exclusively $1/f$ noise behavior ($1.0 \leq \alpha < 1.2$). For large gaps and high frequencies, the thermal noise of the nanojunctions dominates the $1/f$ noise.

6. Obtaining a single molecule junction by closing the gap size

By employing the method of separating the electrodes, one has a greater chance (~50%) of observing an obvious current plateau (corresponding to Au-molecules-Au junction) during the process of breaking the contact. With this technique, the Au-molecule-Au junction formed parallel with the Au-Au junction is more susceptible to being elongated, which results in each break of the Au-molecule-Au definitely showing a plateau after the breaking of Au-Au junction. Thereby, pronounced peaks in the current histogram were always observed with this separating strategy. However in contrast, one only has ~10% chance of observing an obvious current plateau if the approaching electrodes technique is employed. In this case, a direct Au-Au junction may form before the first molecule reaches the opposite electrode due to the roughness of the surfaces of both electrodes, resulting in the absence of a current plateau. Now, let us focus on those curves showing the relevant plateau feature as shown in Figure S5. One can observe that although the jump amplitude and the plateau length was varied from junction to junction, the plateau position indicating the conductance of the molecule junction mainly falls into a long and narrow gray area, as shown in Figure. S5. Also, we can find that the plateau level is comparable to those obtained by the standard separation technique. Therefore, the approaching technique is reproducible and can be used to generate a single molecule junction.

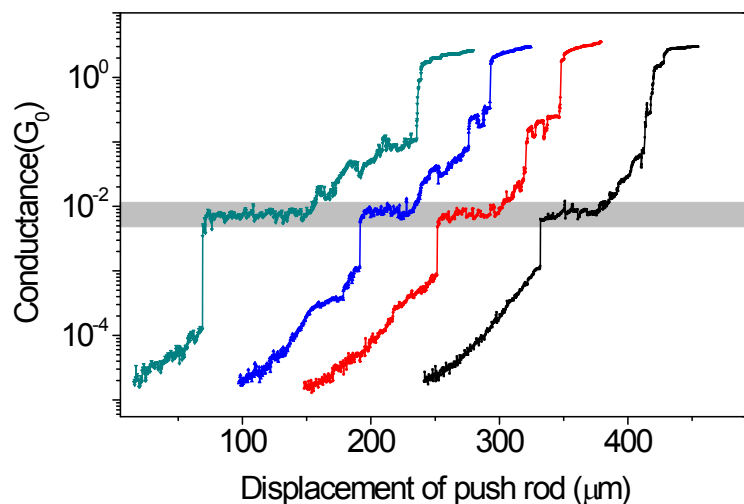


Fig. S5 Conductance change as a function of push rod displacement when employing the approaching electrodes technique. The conductance curves have been shifted in the horizontal direction in order to present them clearly. The voltage $V_B = 0.2$ V was applied to the junction.

7. Determination of the characteristic frequency

In order to discover the position of the characteristic frequency f_0 , we plot $(f \cdot S_V)$ vs f . The vertex of each curve in this plot indicates the position of f_0 , as shown in Fig. S6. It can be found that the characteristic frequency decreased as the length of molecules increased despite the same bond type (Au-NH₂) of the molecular junctions.

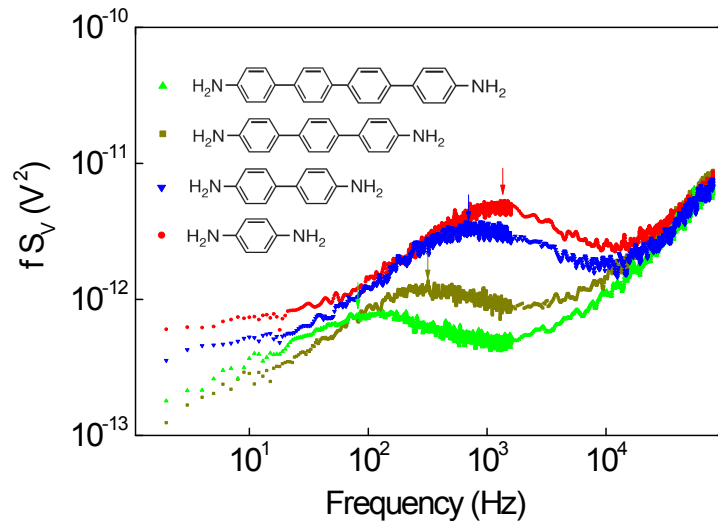


Fig. S6 The voltage noise power spectra of the single-molecule junctions. The characteristic frequency, f_0 , can be obtained by plotting $(f \cdot S_V)$ vs f since the inflection point of each curve indicates the position of the characteristic frequency as indicated by the colored arrows. The characteristic frequency for molecule 1(BDA), molecule 2(DBDA), molecule 3(TBDA), and molecule 4 (QBDA) was found to be 1300 Hz, 720 Hz, 310 Hz, and 90 Hz, respectively.

8. Noise characterization of molecule junctions with differing types of molecules

We also performed more noise spectroscopy measurements of molecular junctions containing a simple backbone (alkane) and strong bond types (Au-S) as shown in Fig. S7. It can be found that a $1/f^2$ noise component (related to the telegram-like fluctuations) exists for the 1,8-octanedithiol molecule. With a strong Au-S bond, it is difficult to break and reconnect to cause current fluctuations. Also, with this simple molecule, the internal phenylene ring rotations are not possible indicating that discrete current fluctuations is unlikely to be caused by ring rotations. Therefore, telegram-like fluctuations are likely to neither originate from the characteristics of the Au-N bond nor from molecule conformational changes.

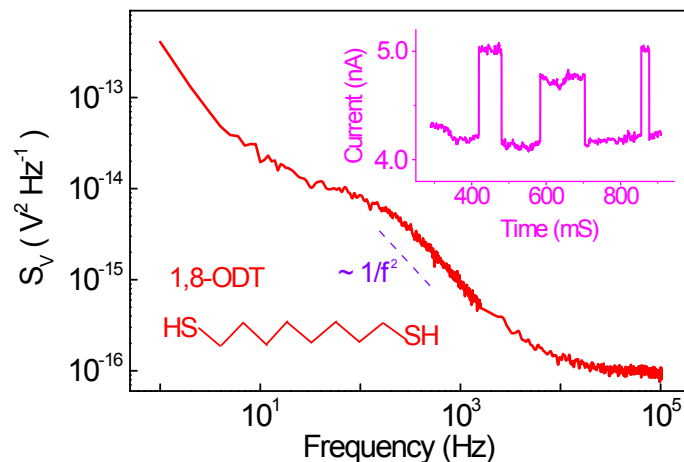


Fig. S7 Noise spectroscopy of single Au-octanedithiol-Au junction. A $1/f^2$ noise component was clearly observed in the recorded spectroscopy. The upper insert is the real-time current fluctuation with an applied bias of $V_B=200$ mV. The lower insert is the schematic drawing of the molecule structure without phenyl rings in the backbone.

9. Telegram-like fluctuations on molecular incubation concentration

To verify the hypothesis that telegraph-like signals originate from the motion of gold atom tethered to a molecule, we compared the switch ratio in different samples with varying molecular coverage densities. To achieve this, the incubation concentration of the molecules was varied from 0.1 to 10 mM when the SAM on the electrode surface was prepared. We observed that for all four types of molecules, the switch ratios were reduced as the incubation concentration increased, indicating that higher molecular coverage ratios hindered the motion of complex species, as shown in Figure.S8.

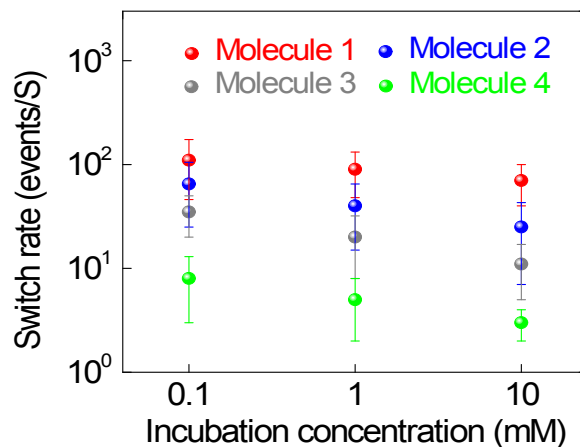


Fig. S8 Telegraph-like switch rate as a function of molecular incubation concentration. This graph demonstrates that the fluctuation rate decreases as the molecular coverage density increases. The average switch ratio and error bar were extracted from 100 real-time current curves, and each of these curves were recorded for the duration of one minute.

References

- S1 L. Grüter, M. González, R. Huber, M. Calame, C. Schönenberger, *Small*, 2005, **1**, 1067.
- S2 J. Reichert, *et al.*, *Phys. Rev. lett.*, 2002, **88**, 176804.
- S3 C. Zhou, *et al.*, *Appl. Phys. Lett.*, 1995, **67**, 1160.
- S4 S. A. G.Vrouw, *et al.*, *Phys. Rev. B.*, 2005, **71**, 035313.
- S5 E. H. Huisman, *et al.*, *Appl. Phys. Lett.*, 2011, **109**, 104305.
- S6 D. Xiang, H.Jeong, D. Mayer, T. Lee, *Nano Lett.*, 2013, **13**, 2809.
- S7 Z. Wu, *et al.*, *Phys. Rev. B.*, **78**, 2008, 235421.